Conference on Modelling Fluid Flow (CMFF'15)
The 16th International Conference on Fluid Flow Technologies
Budapest, Hungary, September 1-4, 2015

Different regimes of the flow around a U-beam and their importance for flutter vibrations

Johannes Strecha[4], Sergey Kuznetsov[2], Stanislav Pospíšil[3], Herbert Steinrück[1]

[1] Corresponding Author. Institute of Fluid Mechanics and Heat Transfer, Vienna University of Technology. Getreidemarkt 9, 1060 Vienna, Austria. Tel.: +43 1 58801 32231, Fax: +43 1 58801 932231, E-mail: herbert.steinrueck@tuwien.ac.at
[2] Institute of Theoretical and Applied Mechanics, Academy of Sciences of the Czech Republic. E-mail: kuznetsov@itam.cas.cz
[3] Institute of Theoretical and Applied Mechanics, Academy of Sciences of the Czech Republic. E-mail: pospisil@itam.cas.cz
[4] Institute of Fluid Mechanics and Heat Transfer, Vienna University of Technology. E-mail: johannes.strecha@tuwien.ac.at

ABSTRACT

Vibrations of a slender U-profile in turbulent cross-flow are studied with the aid of 2D-CFD simulations and wind tunnel experiments. The simulations indicate that there are two different patterns of the flow around the stationary U-profile. Vortices form either towards the leeward flange of the profile, or behind its windward flange. The latter vortices move through the cavity of the profile and lead to large fluctuations of the aerodynamic forces. Thus, the flow patterns determine the vibration response of the U-profile. By comparison with wind tunnel experiments it is shown that aspects of either flow pattern are present in the real flow field. Contrary to simulation results the real flow appears to change between either flow pattern. At zero inclination neither flow pattern prevails. Inclining the profile favours one or the other flow pattern. The importance of the inclination angle and the flow pattern becomes apparent when studying free vibrations of a tensioned belt with U-shaped cross section. Positive inclination of the belt leads to more pronounced vibrations than negative inclination.

Keywords: Vortex induced vibrations, Particle Image Velocimetry, CFD Simulations, Free vibrations

NOMENCLATURE

B	[m]	U-profile length
H	[m]	U-profile height
I	[−]	Turbulence intensity
U^*	[−]	Reduced velocity
c_D	[−]	Drag coefficient
c_L	[−]	Lift coefficient
c_M	[−]	Moment coefficient
f_vs	[Hz]	Vortex shedding frequency
f_0	[Hz]	Eigenfrequency
s_v	[m/s]	Flow velocity standard deviation
t	[s]	Flow-time
u_∞	[m/s]	Far-field flow velocity
y	[m]	(Vertical) displacement
y^+	[−]	Wall distance (CFD)
δ	[−]	Logarithmic decrement
ν	[m^2/s]	Kinematic viscosity (air)
ρ	[−]	Air density
φ	[°]	Rotation angle
Re	[−]	Reynolds number
St	[−]	Strouhal number

Subscripts and Superscripts

(P)	Quantity obtained by experiment
(R)	Quantity under the U-flow pattern
(U)	Quantity under the U-flow pattern
max	Maximum of a (field) quantity
0	Constant value
$\ddot{}$	Second time derivative
$\hat{}$	Peak amplitude
$\tilde{}$	Dimensionless quantity

1. INTRODUCTION

Bluff bodies in cross-flow can be excited to vibrations through various mechanisms relevant in different parameter regimes. Among those, vortex induced vibrations can be particularly challenging to study. Vortex formation and decay, a very complex process on its own, interacts with the motion of the body. The intriguing complexity of the flow field can be revealed by Computational Fluid Dynamics (CFD) simulations. Yet, the accuracy of such simulations, especially when studying turbulent flows, has to be questioned and verified by experiments. The author's research focus is to study cross-flow induced vibrations of bluff bodies through CFD simulations. Specifically, vibrations of a prismatic structure with U-shaped cross section with the aspect ratio $B/H = 4.65$ (see Figure 1) are investigated. Such structures are relevant in many industrial applications.

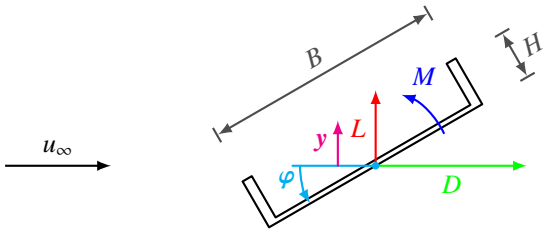

Figure 1. Sketch of the U-profile

Previous two-dimensional (2D) CFD studies of the flow around a statically inclined U-shaped profile lead to the conclusion that there exist two distinct, time-periodic patterns of the flow [1], called U-flow pattern and R-flow pattern. Depending on the inclination angle of the structure different vortex formation patterns would occur. At some inclinations both patterns could be observed through preparation of the initial conditions. Both flow-pattern were metastable in the sense that no spontaneous change of the pattern would occur. Given the complexity of the turbulent flow-field and the restrictive modelling assumptions in the simulation methods a thorough verification of these findings by experiments is required.

The results of this verification are presented in this paper. The investigation relies on the results of 2D-CFD simulations, Particle Image Velocimetry wind tunnel experiments and free vibration experiments involving a tensioned belt with U-shaped cross section. These approaches are detailed in section 2. Comparison between simulated and measured flow fields is given in section 3, wherein the profile is considered to be statically inclined, φ = const. It will be shown that there are indeed different patterns of the flow around the profile, and that the simulations represent a simplified version of the real flow field. The importance of the flow patterns is highlighted in section 4 on the basis of free vibration tests of a tensioned belt at different angles of inclination.

2. METHODS

The experiments were carried out at the Centre of Excellence Telč in the Czech Republic. It has a closed-loop wind tunnel with two closed test-sections, the "aerodynamic" section and the "climatic" section. The former has a cross-section of 1.9 m × 1.8 m and is equipped with honeycombs to reduce the turbulence intensity to about $I = 1\%$. The latter has a cross-section of 2.5 m × 3.9 m but is not equipped with honeycombs [2].

2.1. Particle Image Velocimetry (PIV)

The model for the PIV experiments was made of 5 mm thick perspex and had the dimensions B = 300 mm and H = 60 mm. Its length was 600 mm. It was mounted horizontally in cantilever fashion on an auxiliary plate. The free end was open to not impede the camera's view of the flow-field. A vertical section of the flow field, distanced 300 mm from the auxiliary plate, was illuminated by a LASER from above. Special care was taken to reduce light reflections to a minimum.

The flow field was recorded by a *Dantec Flow Sense EO* camera with a resolution of 2048 × 2048 pixels and analysed with the *Dantec DynamicStudio* version *3.31*. Data presented in this paper was obtained by applying the *Adaptive Correlation* method with a final interrogation area size of 64 px × 64 px overlap 0.5, followed by a 3 × 3 spatial moving average filter. The camera's optical axis was pointing towards the center of the horizontal plate of the model. In the sample image in Figure 2 the model's cross-section is indicated (red). The regions indicated by the blue rectangles contain shadows cast by the glued edges of the model. Contrast there is low and the results are inaccurate. The blue rectangles are shown in every figure showing a flow-field obtained by PIV.

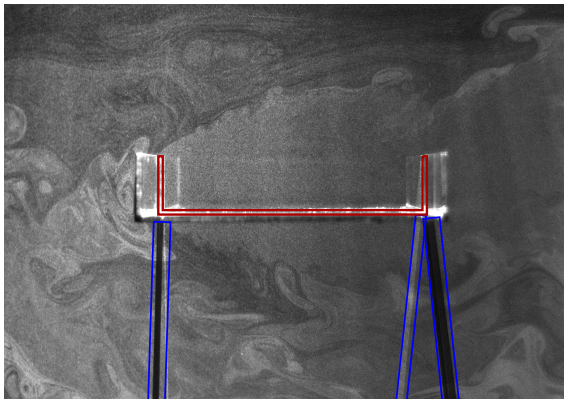

Figure 2. Sample image acquired during the PIV experiments.

Additionally the wake was studied with the help of a CTA probe. The flow velocity magnitude was several locations at the distance B behind the model. These measurements were used to obtain the vortex shedding frequency f_{vs} which is in turn used to calculate the Strouhal number $\mathrm{St} = f_{vs}H/u_\infty$.

2.2. Deformable belt

The experiments involving the tensioned belt were carried out in the "climatic" section of the wind tunnel because of its larger cross-sectional area. The model was made of a rubber band, reinforced with 22 steel cables (diameter 2.9 mm). They were tensioned with a hydraulic cylinder. The sidewalls of the belt were made of non-reinforced rubber. The cross-section of the belt had the same dimensions as the PIV model (B = 300 mm, H = 65 mm). The belt was 2.25 m long. The mass and torsional moment of inertia per unit length were 5.43 kg/m and 0.190 kg m^2/m, respectively. The equilibrium angle of inclination could be adjusted by rotating the belt's fixation on the frame. The acceleration of the belt was recorded by two capacitive, uni-axial accelerometers. They were placed at the half height on either side of the model (see Figure 3). The acceleration signals $\ddot{y}_1$ and $\ddot{y}_2$ were integrated twice in

Fourier space to obtain the belt displacement y_1 and y_2. Due to the non-existent honeycombs in the "climatic" section of the wind tunnel, the turbulence intensity reached levels of about $I = 10\,\%$.

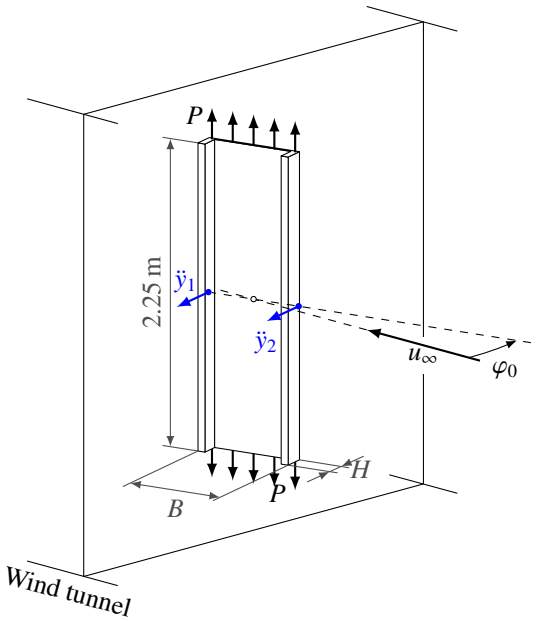

Figure 3. Sketch of the tensioned belt experiment

When the tensioning force 14.2 kN was applied, the lowest eigenfrequencies of the belt were $f_{0,y} = 11.4\,\text{Hz}$ and $f_{0,\varphi} = 10.8\,\text{Hz}$ (pertaining to mode-1 heave and pitch motion). With this tensioning force the logarithmic decrements pertaining to the heave and pitch mode were $\delta_y = 0.021$ and $\delta_\varphi = 0.029$, respectively. The flow conditions in the experiment will be characterised by the dimensionless, so-called reduced velocity. It is the far-field flow velocity u_∞ scaled with the product of the profile height H and the pitch eigenfrequency $f_{0,\varphi}$: $U^* = u_\infty / H f_{0,\varphi}$.

2.3. CFD Simulations

The 2D-CFD simulations were performed using the commercial CFD software package *Ansys Fluent*, version *14.5*. The flow-field was calculated in a rectangular, two-dimensional computational domain and unsteady RANS (URANS) models were used (specifically: the $k\omega$-SST model). The calculation mesh contained approximately $57 \cdot 10^3$ quadrilateral cells, $22.8 \cdot 10^3$ of which are in a region of diameter $2.2B$ centered around the profile. The velocity inlet was placed at a distance $7.7B$ upstream of the profile, the outflow boundary $16.9B$ downstream. Either symmetry boundary at the top and bottom of the domain had a vertical distance of $9.2B$ to the profile. In the wall regions $y^+ \sim 1$ was achieved, implying that low-Reynolds formulations of the wall functions were used. Only second order discretisations were used. At the inlet boundary a free-stream turbulence intensity of $I = 1\,\%$ and an eddy viscosity ratio of 1 were specified.

3. FLOW PATTERNS

The flow fields obtained by simulation will be compared with PIV results. The simulations were carried out at a Reynolds number $\text{Re} = u_\infty B/\nu = 2.45 \cdot 10^5$. In the PIV experiments $\text{Re} = 4.3 \cdot 10^4$ could be reached. The turbulence intensity of the oncoming flow was $I = 1\,\%$ in both cases. Neither the PIV nor the simulations fully resolve the turbulent fluctuations of the flow. In the simulation most fluctuations are modelled through their contribution to the turbulent kinetic energy. The PIV method does not resolve structures smaller than the size of an interrogation area.

The available data consists of the time-periodic flow-fields under either flow patterns obtained by 2D-CFD simulation, and flow-field snapshots obtained by PIV. Meaningful comparison of this data requires a careful approach and will be made in two steps. First, the time-averaged flow fields will be compared. Then snapshots of the flow field will be discussed. Finally the influence of the inclination angle is discussed. The structure is at rest throughout this section, $y \equiv 0$ and $\varphi = \text{const}$.

3.1. Time-averaged flow fields

As a first step the statistics of the flow-field are analysed, i.e. the time-average and standard deviation of the flow velocity. The flow fields obtained by PIV experiments and 2D-CFD simulations are compared. Flow field statistics from PIV data were obtained using one complete series of captured flow field snapshots, which includes estimated 9.5 flow periods, i.e. the sampling time was 9.5 times the vortex shedding frequency under the R-flow pattern, $t_s = 9.5/f_{vs}$. Statistics from simulations were calculated using only one flow period, since the simulated flow is time-periodic.

In Figure 4 the flow-field is visualised by arrows oriented in the direction of the time-averaged flow velocity and scaled by the local velocity magnitude. Additionally, an iso-line of the velocity magnitude standard deviation at the value $0.5\,s_{v,\max}$ is marked (red), where $s_{v,\max}$ is the maximal standard deviation in the field. Areas of large velocity standard deviation indicate regions where the flow is strongly time-dependent. Also note the regions in Fig. 4 where the PIV result is inaccurate (blue rectangles). In the time-averaged flow-field in Fig. 4 a single vortical structure rotating clockwise can be seen above the leeward half of the cavity. However, this region is also characterised by a large velocity standard deviation, indicating a time-dependent and flow field. Below, these regions will be further discussed by snapshots. Furthermore the evolution of the free shear layer separating from the bottom windward corner of the profile is strongly time-dependent and, naturally, the wake behind the profile. The maximal value of the flow velocity standard deviation, scaled with the far-field flow velocity u_∞ was $s^{(P)}_{v,\max}/u_\infty = 0.46$.

Simulation results of either flow pattern are

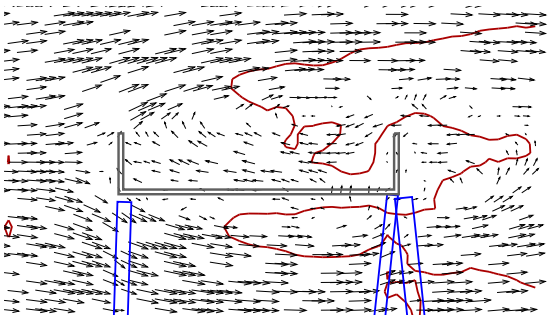

Figure 4. Time-averaged flow field (arrows) with an isoline of the velocity magnitude standard deviation (red), obtained by PIV.

shown in Figure 5. The time-averaged flow-field of the U-flow pattern is characterised by a single, large vortical structure in the cavity of the profile (Fig. 5a), rotating clock-wise. This structure is part of a time-dependent region of the flow-field, as indicated by the red standard deviation contour at $0.5 s^{(\mathrm{U})}_{\mathrm{v,max}}$. In fact, it encompasses the whole cavity, as well as the wake of the profile. The maximal, non-dimensional standard deviation was $s^{(\mathrm{U})}_{\mathrm{v,max}}/u_\infty = 0.94$, including the contribution from the turbulent kinetic energy.

Unlike the previously discussed flow fields the time-averaged R-flow field (Fig. 5b) is characterised by two vortical structures in the cavity of the profile. One vortex in the leeward half of the cavity is rotating in clockwise direction while the other vortex in the windward half of the cavity is rotating in counter-clockwise direction. Note that the standard-deviation iso-line at $0.5 s^{(\mathrm{R})}_{\mathrm{v,max}}$ (where $s^{(\mathrm{R})}_{\mathrm{v,max}}/u_\infty = 0.57$), which already includes the contribution from the turbulent kinetic energy, encompasses only the wake of the profile and a small region in the free shear layer above the cavity and not the two vortical structures.

No conclusive evidence for either flow pattern can be obtained by comparing the time-averaged flow fields. The standard deviations as seen in the PIV data indicate that the flow-field becomes instationary well before the leeward corners of the profile (Fig. 4). Yet, the instationary regions of the U-flow field begins right after the windward flange of the profile. The instationary regions of the R-flow field encompass mainly the wake and it appears that the flow in the cavity and above is almost stationary. The next section discusses snapshots of the flow-field in the light of the already gained insights.

3.2. Flow-field snapshots

First, snapshots of the R-flow pattern are discussed. Investigation of all snapshots during a flow period shows that the two vortices in the cavity are indeed stationary. The topology of the flow field in the cavity does not change. Hence the temporal statistics previously discussed show a very small flow velocity standard deviation. A snapshot of the flow-field under the U-flow pattern is shown in Figure 6. Observe the similarity of the flow-field in the cavity between this figure and Fig. 5b. Yet, the profiles of the horizontal flow velocity component suggest that the free shear layer is sensitive to small perturbations by. Especially the local velocity profile at $x = -0.32B$ (blue, left profile in Fig. 6) resembles that of the shear layer in a Kelvin-Helmholtz scenario. Indeed, the large values of the turbulence intensity I (estimated from the turbulent kinetic energy, magenta line) indicate that many eddies are formed in the free shear layer. These eddies are not resolved in space and time, but accounted for through the turbulent kinetic energy. Larger vortices, present in the wake of the profile are resolved in space and time. The clear distinction between the resolved and modelled timescales is an implicit assumption of URANS models. Critics of URANS methods argue that the evolution of free shear layers may depend sensitively on small eddies and that the implied separation of timescales is not given in bluff body flows [3].

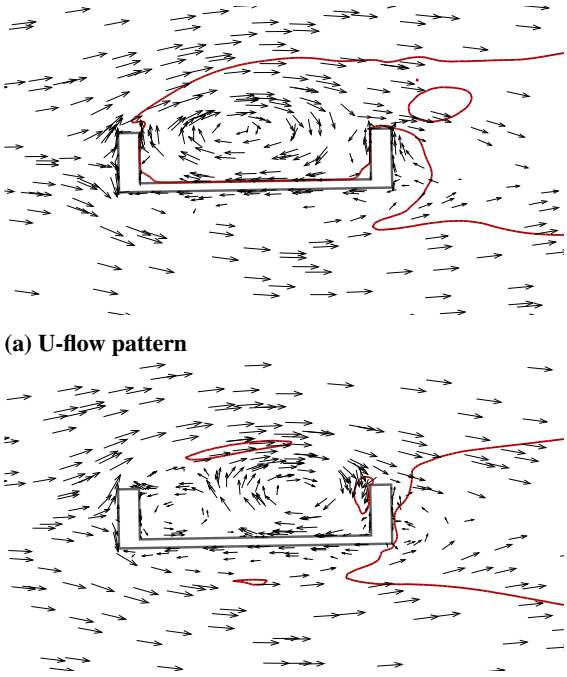

(a) U-flow pattern

(b) R-flow pattern

Figure 5. Time-averaged flow field (arrows) with an isoline of the velocity magnitude standard deviation (red), obtained by CFD Simulation.

Recall, that the U-flow pattern revealed a strongly time-dependent flow-field in the cavity (Fig. 5a). Indeed, a snapshot of the flow-field shows that unlike under the R-flow pattern, the average flow-field has very little in common with a snapshot (Figure 7). By the velocity profile (blue) it can be seen that the free shear layer rolled up right behind the windward flange of the profile to form a vortex rotating in clockwise direction (the “cavity vortex”). Inspection of flow field snapshots shows that this vortex is not stationary. It grows, detaches from the windward flange, travels through the cavity, and is swept over the leeward flange into the wake. The

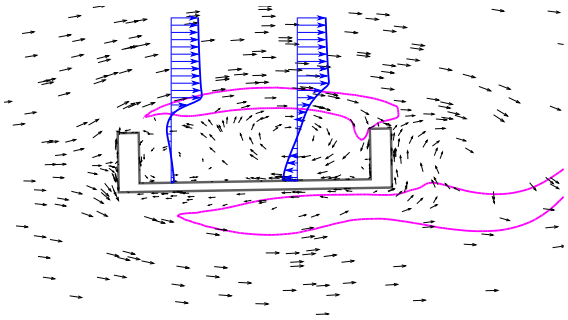

Figure 6. Snapshot of the simulated flow-field (R-flow pattern) with two u-velocity profiles and a turbulence intensity isoline, I = 15 %.

green arrow in Fig. 7 shows the approximate path of the vortex core. The vortex at the tip of the arrow was formed behind the windward flange (where the green arrow begins) during the previous flow period and has travelled towards the leeward flange. The turbulence intensity is low where the cavity vortex forms but large between the two vortical structures, and also around the shear layer below the profile.

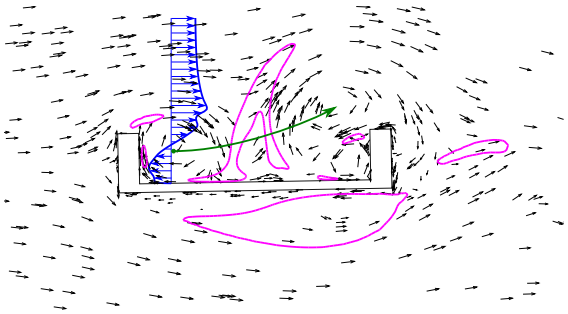

Figure 7. Snapshot of the simulated flow-field (U-flow pattern) with a u-velocity profile and a turbulence intensity isoline, I = 15 %.

Another often stated criticism of URANS methods, especially in two-dimensional computational domains, is the slow decay of vortical structures as they travel through the computational domain. The large turbulence intensities around the second vortex in Fig. 7 suggest that the (three-dimensional) decay of the cavity vortex may be important in reality. Before the influence of the cavity vortices on the aerodynamic forces is discussed, a comparison with snapshots of the flow field obtained by the PIV experiments is given, where evidence for the cavity vortices will be given.

Some snapshots of the flow-field resemble the aforementioned R-flow patterns in a way (see Figure 8). The shear-layer is curved weakly and reaches over the cavity of the profile (green arrows). Vortices can be seen in the wake behind the profile. The flow in the cavity itself does not resemble the R-flow pattern. Instead, the orientation of the arrows suggest a three-dimensional flow-field. Despite this, the velocity profile (blue) is similar to the profile shown in Fig. 6, locally resembling a Kelvin-Helmholtz Scenario. In parallel shear-flows such a velocity profile could be unstable by Fjørtoft's criterion [4]. Indeed, a vortex of considerable size can be seen in this snapshot to the right of the velocity profile (green arrows). These vortices were modelled as a contribution to the turbulent kinetic energy in the simulations under the R-flow pattern (see Fig. 6). The question is whether these vortices can take on the role of the cavity vortex, which is observed in 2D-CFD simulations under the U-flow pattern.

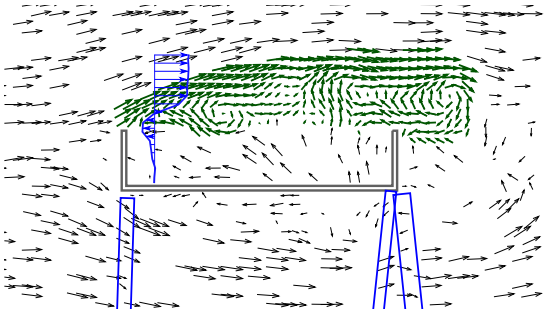

Figure 8. Snapshot of the flow-field (PIV), visualised by arrows and a u-velocity profile. The shear layer is curved weakly.

There is evidence that vortices can form right behind the windward flange of the profile (see Figure 9, green arrows). By the u-velocity profile (blue) it can be seen that a clockwise-rotating vortex is located at this position. Under the R-flow pattern a counter-clockwise rotating vortex would be present. This vortex is not stationary, but travels through the cavity towards the leeward flange. Also in Fig. 9 a second vortex rotating in clockwise direction can be seen at this position (green arrows). Subsequent snapshots show the left vortex detaching from the windward flange and travelling towards the leeward flange [5]. Furthermore it can be observed that many vortical structures are located below the profile. These were also modelled as a contribution to the turbulent kinetic energy in the simulations.

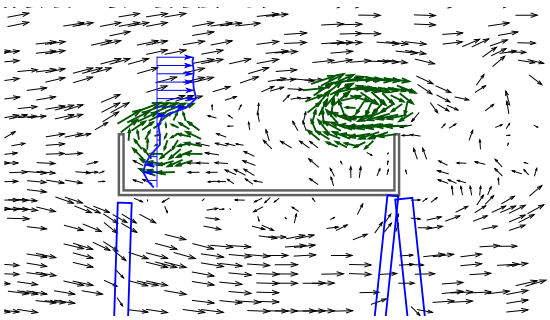

Figure 9. Snapshot of the flow-field (PIV), visualised by arrows and a u-velocity profile. A cavity-vortex has formed.

Thus, aspects of both flow patterns were observed at the same angle of inclination in the PIV experiments. The Figs 8 and 9 show only two out of 44 recorded flow-field snapshots. These snap-

shots were analysed how closely they resemble either the U-flow or the R-flow pattern. It was chosen to count snapshots where vortices rotated in counter-clockwise direction in the windward half of the cavity as "R-flow frame". Frames where clockwise rotating vortices were located in the cavity of the profile were considered an "U-flow frame". All other frames were counted as "undecidable". Of 44 frames spanning 19 flow periods, 13 frames resembled the U-flow pattern by the above described criteria. Only one was considered to represent the R-flow pattern. The remaining 30 frames were deemed "undecidable". These frames are mainly characterised by small vortices forming in the free shear layer and a possibly three-dimensional flow in the cavity (similar to Fig. 8). The two almost stationary vortices seen in 2D-CFD simulations under the R-flow pattern (Fig. 5b) could be unstable in three dimensions. Thus, the "undecidable" frames may resemble the R-flow pattern. Then, the flow switches between two bi-stable states corresponding to the flow patterns observed in 2D-CFD simulations. The simulations show no intermittent change between the flow patterns. Change between flow patterns from U-flow to R-flow and back again could only be achieved by substantially varying the inclination angle during a simulation run.

3.3. Aerodynamic forces

In this section the aerodynamic forces acting on the U-profile will be discussed on the basis of simulation results. The drag and lift force and torsional moment per unit length are given by $c_{\mathrm{D|L}} \frac{1}{2}\rho u_\infty^2 H$ and $c_{\mathrm{M}} \frac{1}{2}\rho u_\infty^2 HB$, respectively. They were obtained from simulations at the same Reynolds-Number $\mathrm{Re} = 2.45 \cdot 10^5$ as in the flow-field snapshots above. Since the flow is turbulent and considered to be periodic, a time-series of aerodynamic forces obtained by URANS simulation can be thought of as the so-called *phase average*. Note that the time-periodicity of the flow is contradicted by the PIV experiments and that the following figures are used to illustrate the influence of the cavity vortices only.

The time-series of the aerodynamic forces under the R-flow pattern are almost sinusoidal (Figure 10). The oscillation frequency equals the vortex shedding frequency. Vortices are formed in the wake of the profile (Fig. 6) and do not impinge upon any part of the profile. The lift coefficient is always positive and the coefficient of torsional moment oscillates with an amplitude of $\hat{c}_{\mathrm{M}} = 0.13$.

The aerodynamic forces under the U-flow pattern show much more features (Figure 11). Most importantly, the U-flow pattern leads to a different fundamental frequency of the aerodynamic forces than under the R-flow pattern (note the scale of the time-axis in Figs. 10 and 11). Under the U-flow pattern, the influence of the vortex formation in the wake is much less important than the influence of the cavity vortex. Inspection of snapshots of the flow-field

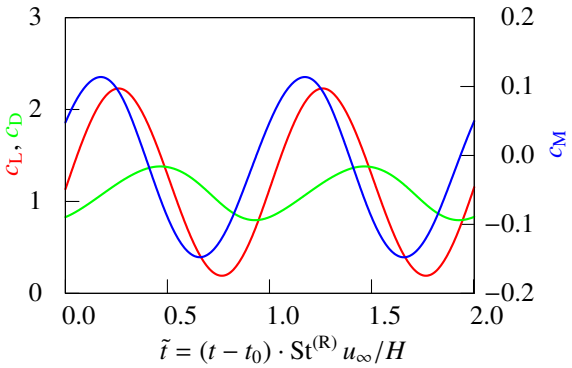

Figure 10. Time-series of the aerodynamic force coefficients under the R-flow pattern (simulation at $\varphi = 0°$)

leads to the following conclusions: The drag coefficient is the greatest when a cavity vortex is swept into the wake ($\tilde{t} \approx 0.25$). At the same time, the lift coefficient is negative and almost assumes its minimal value. The coefficient of torsional moment also assumes its minimum then. Maximum lift occurs when the cavity vortex has detached from the windward flange and is in the middle of the cavity ($1.1 \lesssim \tilde{t} \lesssim 1.7$). The coefficient of torsional moment is large in this interval and assumes its maximum shortly before the cavity is swept into the wake. It oscillates with an amplitude of $\hat{c}_{\mathrm{M}} = 0.63$.

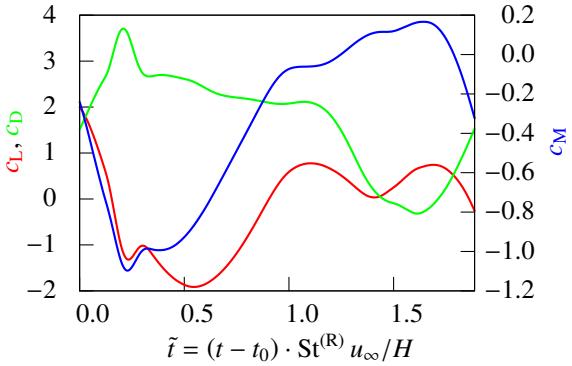

Figure 11. Time-series of the aerodynamic force coefficients under the U-flow pattern (simulation at $\varphi = 0°$)

Thus, the fundamental frequency of the aerodynamic forces is given by the speed at which the vortex travels through the cavity of the profile. In the simulations this travelling speed is rather slow so that the flow period under the U-flow pattern is almost twice as large as under the R-flow pattern, $\mathrm{St}^{(\mathrm{R})} \approx 2\mathrm{St}^{(\mathrm{U})}$. Inspection of the PIV snapshots yields that this timing is almost correct. In one instance $\mathrm{St}^{(\mathrm{P,U})} = 1.95^{(\mathrm{P,R})}$ was obtained: $\mathrm{St}^{(\mathrm{P,U})}$ was determined from three successive frames showing cavity vortices. $\mathrm{St}^{(\mathrm{P,R})}$ was obtained from the frequency spectrum of the velocity magnitude measured behind the profile with a CTA probe. At this inclination, $\mathrm{St}^{(\mathrm{P,U})}$ could not be determined reliably from CTA

data. Cavity vortices form irregularly and are subject to three-dimensional decay.

3.4. Influence of the angle of inclination

The flow around statically inclined U-profiles was also investigated by means of PIV measurements. First, let the U-profile be positively inclined, $\varphi_0 = 5°$. Application of the criteria described above lead to the following results: Of 44 available snapshots none resembled the R-flow pattern but 26 showed features of the U-flow pattern. The remaining 18 snapshots were deemed undecidable. When positively inclined, the leeward flange of the profile is closer to the free shear layer and influences the formation of cavity vortices such that they appear more often. Inspection of the flow velocities in the wake behind the U-profile by means of a CTA probe showed that there is a band of frequencies present, yielding $0.065 \leq \mathrm{St}^{(\mathrm{P,U})} \leq 0.083$. These frequencies correspond to the formation of cavity vortices. They are lower than the Strouhal number attributed to the "classical" vortex shedding $\mathrm{St}^{(\mathrm{P})} = 0.133$, obtained at $\varphi_0 = 0°$, and also lower than the Strouhal numbers others observed in the flow around a rectangular prisms with similar aspect ratio [6].

When the U-profile is negatively inclined, $\varphi_0 = -5°$ none of the 44 available snapshots resemble either U-flow or R-flow pattern. Instead, every frame is "undecidable" by the above described criteria. The snapshots are characterised by a very complex flow in the cavity which appears to be non-periodic and highly three-dimensional. The shear layer separating from the top windward corner of the profile is still easily perturbed and forms vortices. Yet they move above the leeward flange and do not influence the flow in the cavity much. Inspection of the flow velocities in the wake yield a Strouhal number $\mathrm{St}^{(\mathrm{P})} = 0.133$ which is numerically equal to the value of St obtained at zero inclination $\varphi_0 = 0°$.

Changing the angle of inclination in the simulations leads to similar results. At a positive inclination $\varphi_0 = 5°$ or negative inclination $\varphi_0 = -5°$ vortices form according to the U-flow pattern or the R-flow pattern, respectively. The topology and character of the flow at either angle is equal to the corresponding pattern at zero inclination.

4. FLOW INDUCED VIBRATIONS

In this section the relevance and influence of the cavity vortices for flow induced vibrations will be shown by discussing the influence of the angle of inclination on the vibration amplitudes. The vibration amplitudes in Figure 12 are given as the minimal and maximal average peak amplitude: The values of ten consecutive local maxima of the displacement signal were averaged to obtain one average peak amplitude. With an overlap of five consecutive maxima the next portion of the signal, again containing ten consecutive local maxima, was analysed. The minimal and maximal average peak amplitude was stored and used to plot the bars in the figure. The experiments described here were carried out with a single belt eigenfrequency of $f_{0,\varphi} = 11.4\,\mathrm{Hz}$. The reduced velocity U^* was varied by changing the far-field flow velocity u_∞. The Reynolds number range was $2.0 \cdot 10^5 < \mathrm{Re} < 4.5 \cdot 10^5$ in these experiments.

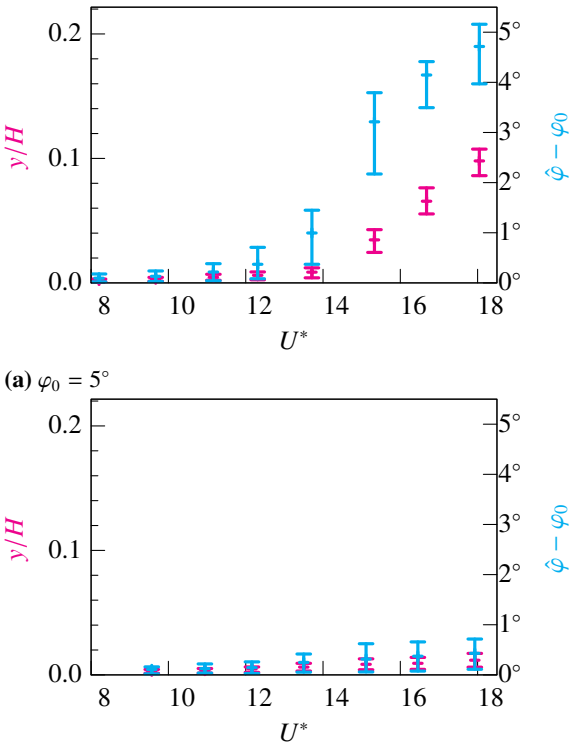

(a) $\varphi_0 = 5°$

(b) $\varphi_0 = -5°$

Figure 12. Dimensionless heave and pitch motion at several reduced velocities and two base inclinations φ_0.

At positive inclination $\varphi_0 = 5°$ (Fig. 12a) vibration amplitudes stay small for reduced velocities up to $U^* = 12$. From there on the pitch amplitude increases to values up to $\hat{\varphi} - \varphi_0 \approx 5°$. The heave amplitudes also increase, but appear to be less important than the pitch motion. Recall, that the peak amplitude of the coefficient of torsional moment was almost five times larger under the U-flow pattern than under the R-flow pattern. The reduced velocity from which on vibration amplitudes increase, $U^* = 14$, corresponds to the formation frequency of cavity vortices observed in the simulations under the U-flow pattern. Taking the inverse of the Strouhal numbers at the constant, positive inclination $\varphi = 5°$ leads to an estimate of the critical velocity $12.0 \leq U^* \leq 15.4$. Since vibration amplitudes increase until the largest achieved reduced velocity, $U^* \approx 18$, the lock-in range of the cavity vortices appears to be rather large, or another instability mechanism is in effect.

At negative inclination $\varphi_0 = -5°$ (Fig. 12b) vibration amplitudes stay small for all investigated reduced velocities, $\hat{\varphi} - \varphi_0 < 1°$. If there were vortex induced vibrations at $U^* \approx 7.5$, the corresponding

lock-in range has to be rather small since vibration amplitudes at $U^* \approx 9.5$ are minimal.

5. CONCLUSIONS AND OUTLOOK

Two time-periodic flow pattern were observed in 2D-CFD simulations of the flow around a profile with U-shaped cross-section. By thorough comparison with data obtained by PIV experiments it was confirmed that aspects of both flow patterns are present in the flow-field. The intermittent change of flow patterns, observed in the experiments, is not unique to the flow around a U-profile. Such phenomena are also reported by Tamura and Itoh in their study of the flow around a short rectangular prism [7]. There, the flow patterns are related to the either weak or strong roll-up of a shear layer behind a short rectangular prism with $B/H = 0.2$. In the present case the shear layer roll-up is also relevant, but it is the formation of cavity vortices brought on by the strong shear layer roll-up that is thought to be the defining aspect of the U-flow pattern. It was shown that these cavity vortices have a tremendous influence on the aerodynamic forces acting on the profile. Such cavity vortices (or "surface travelling vortices") were observed by Kubo et al in their experimental study of the flow around an H-shaped prism with an aspect ratio of $B/H = 10$, [8]. Kubo et al also indicated that the formation of cavity vortices can be influenced by forcing the profile to move. This further underlines the importance for vibration excitation by the cavity vortices since it confirms that the vortex formation synchronises to the profile motion. Furthermore, the velocity spectra obtained by CTA measurements of the wake behind the statically inclined profile show that the formation of cavity vortices does not take place at a single, well defined frequency but rather in an interval of frequencies. This also indicates that the formation frequency is not a given constant but that it can change.

As a way to investigate the importance of the cavity vortices for flow induced vibrations, vibrations of a tensioned belt at different base inclinations were studied. At negative base inclination vibration amplitudes were very low in general. At positive inclination vibrations set in at a reduced velocity which is be related to the cavity vortex formation frequency. The importance of such vortices for flow induced vibrations is also highlighted by others [8, 9].

Comparison of simulated and calculated (PIV) flow fields shows that the simulation methods need more attention in future research. While the applied URANS methods are computationally feasible, they yield "simplified" results. The flow patterns are time-periodic and the intermittent change cannot be predicted. Due to [3] there is considerable doubt that extending the computational domain to three dimensions but using the same turbulence model would lead to more accurate results. An estimate for the computational cost of an LES simulation of the present case, based on grid resolutions in [6], leads to the conclusion that pure LES is prohibitively expensive. Scale Adaptive Simulations are considered as option.

ACKNOWLEDGEMENTS

The support of the Czech-Taiwan research project GAČR No. 13-24405J and NSC101WFD0400131 as well as the support of LO1219 - Sustainable advanced development of CET and RVO 68378297 is gratefully acknowledged.

REFERENCES

[1] Strecha, J., and Steinrück, H., 2014, "Dependence of the aeroelastic stability of a slender U-beam on the realized flow pattern", *PAMM*, Vol. 14 (1), pp. 497–498.

[2] "Climatic Wind Engineering Laboratory | Centre of Excellence Telč", URL `http://cet.arcchip.cz/wind-laboratory-en`, Accessed on 2015-02-18.

[3] Fröhlich, J., and von Terzi, D., 2008, "Hybrid LES/RANS methods for the simulation of turbulent flows", *Progress in Aerospace Sciences*, Vol. 44 (5), pp. 349–377.

[4] Drazin, P. G., 2002, *Introduction to Hydrodynamic Stability*, Cambridge University Press, ISBN 978-0-52-100965-2.

[5] Strecha, J., In preparation, "Flow induced vibrations of a slender U-beam (working title)", Ph.D. thesis, Vienna University of Technology, supervisor: Prof. Herbert SteinrÃijck. Second Examiner: Stanislav Pospíšil.

[6] Mannini, C., Šoda, A., and Schewe, G., 2011, "Numerical investigation on the three-dimensional unsteady flow past a 5:1 rectangular cylinder", *Journal of Wind Engineering and Industrial Aerodynamics*, Vol. 99 (4), pp. 469–482.

[7] Tamura, T., and Itoh, Y., 1999, "Unstable aerodynamic phenomena of a rectangular cylinder with critical section", *Journal of Wind Engineering and Industrial Aerodynamics*, Vol. 83 (1–3), pp. 121–133.

[8] Kubo, Y., Hirata, K., and Mikawa, K., 1992, "Mechanism of aerodynamic vibrations of shallow bridge girder sections", *Journal of Wind Engineering and Industrial Aerodynamics*, Vol. 42 (1–3), pp. 1297–1308.

[9] Matsumoto, M., Shirato, H., Yagi, T., Shijo, R., Eguchi, A., and Tamaki, H., 2003, "Effects of aerodynamic interferences between heaving and torsional vibration of bridge decks: the case of Tacoma Narrows Bridge", *Journal of Wind Engineering and Industrial Aerodynamics*, Vol. 91 (12–15), pp. 1547–1557.